Journal of Catalysis **194,** 301–308 (2000)
doi:10.1006/jcat.2000.2936, available online at http://www.idealibrary.com on IDEAL®

Kinetics of Isobutane Dehydrogenation and Cracking over HZSM-5 at Low Pressures

Sun Yanping and Trevor C. Brown

Chemistry, School of Physical Sciences and Engineering, University of New England, Armidale, New South Wales, Australia
E-mail: t.brown3@metz.une.edu.au

Received January 31, 2000; revised May 19, 2000; accepted May 24, 2000

Isobutane cracking and dehydrogenation over HZSM-5 have been investigated under conditions where gas-phase collisions are minimized. The experimental vacuum system consists of a low-flow leak value, two interchangeable, thermally heated reactors (volumes = 8700 ± 5 mm^3 and 2114 ± 5 mm^3), each with a small exit aperture (effective areas = 0.16 mm^2 and 0.37 mm^2), and a quadrupole mass-spectrometer detector. The flow rate, reactor, and exit aperture dimensions are crucial to the kinetic analysis and have been accurately measured. For kinetic measurements the temperature of the reactor is heated at a constant rate from 200–500°C to minimize heat fluctuations, which can result from nonequilibrium adsorption at reaction temperatures, and to obviate the need for an internal standard. Cracking and dehydrogenation reaction channels dominate isobutane decomposition over the temperature range. Propene and methane formation are more prevalent than isobutene evolution. The rate constant for cracking is

$$k_{2a}(^{\circ}\mathrm{C}^{-1}) = 10^{17.3\pm1.1}\exp(-170 \pm 6\ \mathrm{kJ\ mol}^{-1}/RT),$$

and for dehydrogenation it is

$$k_{2b}(^{\circ}\mathrm{C}^{-1}) = 10^{16.8\pm1.1}\exp(-172 \pm 6\ \mathrm{kJ\ mol}^{-1}/RT),$$

Large preexponential factors indicate that the coverage of active sites is less than the coverage of exposed sites available for direct adsorption of isobutane. The similarity in the activation energies for the two channels agrees with theoretically determined proton affinities.

Key Words: **isobutane; catalytic cracking; dehydrogenation; HZSM-5.**

INTRODUCTION

Very low pressure flow reactors have been used extensively to make accurate kinetic measurements of homogeneous gas-phase reactions (1). Heterogeneous gas–solid processes have also been successfully investigated, under molecular flow conditions, but most studies have been on low-temperature reactions or on the effects of various surfaces on gas-phase pyrolysis (1–3). Studies on the kinetics of higher-temperature catalytic reactions at very low pressures are lacking. In very low pressure flow reactors, gas/wall collisions dominate over gas/gas collisions. As a consequence, primary and secondary gas-phase reactions are minimized and the gas/wall collision frequency may be accurately calculated. Adjusting either the surface-to-volume ratio of the cell or the cell's exit aperture varies the collision frequency. Gas-phase species emanating from the cell are monitored by mass spectrometry, or by laser-based optical detection (3).

A wide range of temperature-programmed reaction spectroscopy (TPRS) methods have been used to qualitatively characterize catalysts and, in some cases, to extract kinetic data (4). The simplest and most commonly used TPRS method is to monitor a chemical reaction while the temperature is increased linearly in time. Advantages of this method are that

(i) large temperature fluctuations are avoided at reaction temperatures as exothermic adsorption is allowed to reach equilibrium at temperatures where reaction is negligible, and

(ii) a range of temperatures can be investigated over a short period of time, which obviates the need for an internal standard when determining rate parameters (5).

Zeolite-catalyzed hydrocarbon transformations, such as cracking, dehydrogenation, isomerization, alkylation, oligomerization, aromatization, and coking, are of significant economic importance to the petroleum refinery and the petrochemical industry. Zeolites are commonly used because Brønsted and/or Lewis acid sites effectively initiate the transformations and inherent well-defined pore structures enhance selectivity. The present understanding of the mechanism of alkane transformations catalyzed by solid acids has been recently discussed by several authors (6–8).

Adsorbed carbenium ions $[C_nH_{2n+1}]^+$ are generally considered to be crucial intermediates in the reaction scheme. These ions rearrange to more stable species. For cracking, breakage of the C–C bond, located β to the carbon with the positive charge, then occurs, producing an alkene and a

0021-9517/00 $35.00

secondary or tertiary carbenium ion. An alternative pathway is hydride transfer from an alkane to the carbenium ion, producing new alkane and carbenium ion species. These β scission, stabilization, and hydride transfer steps are well accepted, although some details, such as the role of silyl ether or oxonium ions on the surface, are not fully realized (9). Also, theoretical studies (6) have suggested that the accepted mechanisms are oversimplifications. Most crucially, however, there is a lack of experimental evidence for the mechanism of the initial formation of the carbenium ion from an alkane feed (10). The two mechanisms that are most often proposed are (11):

(i) Hydride ions are abstracted from alkanes at Lewis acid sites $[AlO]^+$.

$$C_nH_{2n+2} + [AlO]^+ \rightarrow [C_nH_{2n+1}]^+ + [HAlO]$$

Lewis acid sites form following dehydration of Brønsted acid sites and are dominant at high temperatures (12).

(ii) Carbonium ions form at Brønsted sites then decompose rapidly to the carbenium ion.

$$C_nH_{2n+2} + [HO] \rightarrow [C_nH_{2n+3}]^+ + [O]^-$$
$$[C_nH_{2n+3}]^+ \rightarrow [C_nH_{2n+1}]^+ + H_2$$
$$\rightarrow [C_{n-x}H_{2n-2x+1}]^+ + C_xH_{2x}$$

These initial steps can be distinguished from each other by a characterization of the acid sites and a product analysis; with a careful choice of alkane feed, a predictable range of alkane products can distinguish the mechanisms. For example, 3-methylpentane cracking over HY and HZSM-5 zeolite catalysts was used by Haag and Dessau (13) to show that carbenium ions form via both carbonium ion intermediates and hydride abstraction.

Most previous experimental studies of the mechanism for initial carbenium ion formation have investigated the product distribution under high-pressure conditions where secondary reactions proliferate. Hence observed products may not represent the initial formation of the carbonium or carbenium ion but may result from a series of steps. These steps include those involved in coke formation, which can be a source of observed H_2 (14). In this paper, TPRS is performed under low-pressure (molecular flow) conditions to determine the initial kinetics of cracking and dehydrogenation of isobutane over HZSM-5. Isobutane catalytic decomposition and product formation is monitored under conditions where secondary reactions are minimized. That is, conditions where the pressure is sufficiently low to minimize gas–gas collisions and isobutane coverage on HZSM-5, as well as to limit the number of reactant and product collisions with adsorbed species on the catalyst surface.

EXPERIMENTAL

Figure 1 is a simple representation of the key components of the reaction system. The reactant gas, isobutane for the present study, passes through a variable leak valve (Granville-Phillips, Series 203), through 240 mm of 1-mm-ID capillary glass tubing and into the Pyrex reaction cell containing the catalyst. Isobutane molecules then experience collisions with the walls of the reactor and catalyst bed. Under molecular-flow conditions, the average number of collisions is determined by the reactor and catalyst geometry, prior to the molecules' escape through the exit aperture, directly into a quadrupole mass spectrometer.

The variable leak valve can control gas flow in the range 300 to 10^{-10} Torr L s^{-1}. Flow rate is monitored before each experiment by recording the pressure decrease from the pressure gauge situated, in a known volume, next to the variable leak valve. The capillary tubing, which is tapered to an internal diameter of approximately 0.5 mm at the reactor end, minimizes back-diffusion. This tubing is precisely fitted inside 4-mm-ID tubing, so it can be removed to replace the catalyst. The reactor is located at the center of a tube furnace, with a heated length of 500 mm, and inside a 30-mm-ID vacuum-sealed glass tube. To ensure efficient heat transfer between furnace and catalyst, more than 65% of the reactor is either touching or within 1 mm of the outer tube. A thermocouple is situated outside the vacuum but adjacent to the reactor, and the temperature is maintained by a Eurotherm 2416 temperature controller. The detection system is a Hewlett Packard 5995 quadrupole mass spectrometer and is daily tuned with perfluoro-tert-butylamine. Data from the mass spectrometer computer, which both controls and acquires data, is transferred to a personal computer for kinetic analysis.

Two reactors have been constructed with different volumes and exit aperture areas, resulting in collision numbers that differ by a factor of 6.3. Key details of these reactors are listed in Table 1. Collision number (Z) is calculated from the ratio of the area of the reactor walls (S_v) to the area of the exit aperture (S_{ea}). Measured exit aperture areas have been corrected by Clausing factors (15) (0.202 for Reactor 1 and 0.275 for Reactor 2) to take into account the finite width of the exit aperture. Residence time of the average molecule

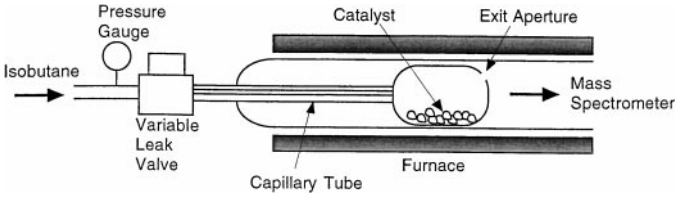

FIG. 1. Diagram of key components of the low-pressure reactor.

TABLE 1

Key Physical Parameters, Calculated in the Absence of a Catalyst, for the Two Reactors

Reactor 1	
Volume	8700 ± 5 mm^3
Internal surface area	2570 ± 2 mm^2
Exit aperture area	0.16 ± 0.03 mm^2
Collisions/molecule	16000 ± 3000
Residence time (s)	$1.5(M/T)^{1/2}$
Reactor 2	
Volume	2114 ± 5 mm^3
Internal surface area	942 ± 2 mm^2
Exit aperture area	0.37 ± 0.03 mm^2
Collisions/molecule	2550 ± 200
Residence time (s)	$0.16(M/T)^{1/2}$

in the reactor is given by (1)

$$t_r = \frac{4V}{S_{ea}}\left(\frac{\pi M}{8RT}\right)^{1/2}, \quad [1]$$

where V is the reactor volume and M is the reactant molar mass. In order to ensure that gas/gas collisions are minimized, the mean free path of the reactant molecules must be greater than the dimensions of the reactor. The largest dimension for both reactors is the length, which is 42 mm for Reactor 1 and 22 mm for Reactor 2. The mean free path is

$$\lambda = \frac{kT}{2^{1/2}\sigma p}, \quad [2]$$

where k is the Boltzmann constant, σ is the collision cross section, which is calculated using the Lennard–Jones diameter of isobutane (5.278 Å) (16), and pressure p is given by (17)

$$p = \frac{dn_{C_4H_{10}}}{dt}\frac{\sqrt{2\pi MRT}}{S_{ea}}. \quad [3]$$

Substituting Eq. [3] into [2] and rearranging gives the flow rate

$$\frac{dn_{C_4H_{10}}}{dt} = \frac{S_{ea}kT}{2\sigma\lambda\sqrt{\pi MRT}}. \quad [4]$$

The maximum isobutane flow rates for the two reactors are when $\lambda = 42$ or 22 mm, so at 200°C for Reactor 1 this corresponds to 6.4×10^{14} molecules s^{-1}, and for Reactor 2 the maximum is 1.2×10^{15} molecules s^{-1}. For all experiments the isobutane pressure in the reactors is in the range 7–10 Pa.

Zeolyst International (Kansas City, USA) supplied the ammonium ZSM-5 powder (CBV 3024G), and conversion to HZSM-5 was achieved by heating in air at 500°C. The original zeolite has a unit cell formula of $NH_{5.48}(Si_{90.52}Al_{5.48})O_{190.9}$ and an N_2 BET surface area of 400 ± 10 m^2 g^{-1}. When necessary the zeolite was quantitatively transferred between reactors, so the same sample was used for all experiments. The mass was 0.2653 g and the particle size was <23 mesh. Isobutane, isobutene, propene, and methane, all instrument grade, were obtained from BOC Gases and were used without further purification.

The method used for temperature-programmed experiments is to expose the reactor, and hence the catalyst, to a flow of isobutane for ca. 2 h at 200°C. At this temperature, where no reaction is apparent, the flow rate is determined. The temperature controller is then programmed to increase the reactor temperature at a constant rate (2, 5, or 10°C/min). This system temperature and mass-spectrum is recorded at regular intervals until the temperature reaches 500°C. In order to remove any coke that may have deposited on the zeolite surface, after each temperature-programmed experiment the catalyst is exposed to a flow of O_2 at 500°C for ca. 16 h.

KINETICS

Mechanism for HZSM-5-Catalyzed Isobutane Decomposition

The mechanism employed to describe the rate-determining steps in the reaction of isobutane over HZSM-5 (HZ) includes adsorption and desorption of isobutane and surface reaction to form products.

$$C_4H_{10} + HZ \underset{k_{-1}}{\overset{k_1}{\rightleftarrows}} HZ(C_4H_{10})_e \quad [R1]$$

$$HZ(C_4H_{10})_a \xrightarrow{k_{2a}} HZ(C_3H_6 + CH_4) \quad [R2a]$$

$$HZ(C_4H_{10})_a \xrightarrow{k_{2b}} HZ(C_4H_8 + H_2) \quad [R2b]$$

Here, $HZ(C_4H_{10})_e$ and $HZ(C_4H_{10})_a$ refer to the coverage of the exposed surface available for direct adsorption of isobutane and the coverage of active sites, respectively. Unimolecular decay of the adsorbed isobutane proceeds via a two-channel process that results in isobutene and hydrogen or propene and methane. In the kinetic model, surface diffusion to or from active sites is assumed to be rapid and hence not rate determining. Reported activation energies for intracrystalline diffusion of isobutane on HZSM-5 and silicalite range from 23.4 to 28.9 kJ mol^{-1} (18, 19), while a typical preexponential factor for surface hopping is 3×10^9 s^{-1} (20). Over the temperature range 200 to 500°C these parameters yield rate constants of the order 4×10^6 to 3×10^9 s^{-1}. Although surface coverage is low, under the low-pressure conditions of the experiment, the diffusion rate is significantly faster than reaction or adsorption rates.

Rate of HZSM-5-Catalyzed Isobutane Decomposition

For unimolecular decay of the surface species the rate expression is

$$\frac{dn_{Product}}{dT} = \frac{k_{2a\text{ or }2b}}{\beta}\theta_{C_4H_{10},a}, \quad [5]$$

where $\theta_{C_4H_{10},a}$ is the coverage of isobutane on the active surface of the zeolite and β is the heating rate. The coverage is estimated by assuming that a steady state is achieved among isobutane adsorption, desorption, and reaction, prior to escaping from the reactor and entering the mass spectrometer chamber. That is,

$$\frac{d\theta_{C_4H_{10},a}}{dt} = k_1 P_{C_4H_{10}} - k_{-1}\theta_{C_4H_{10},e} - k_{2a}\theta_{C_4H_{10},a} - k_{2b}\theta_{C_4H_{10},a} = 0. \quad [6]$$

Here the approximation is made that coverage of the exposed HZSM-5 surface ($\theta_{C_4H_{10},e}$) is equal to $\theta_{C_4H_{10},a}$. This is accurate if the rate constant for surface diffusion to active sites is large and equal to the rate constant for diffusion from active sites. After rearrangement of Eq. [6], the following expression for active-site coverage is obtained:

$$\theta_{C_4H_{10},a} = \frac{k_1 P_{C_4H_{10}}}{k_{-1} + k_{2a} + k_{2b}}. \quad [7]$$

Substituting Eq. [7] into Eq. [5] gives

$$\frac{dn_{Product}}{dT} = \frac{k_{2a\text{ or }2b}}{\beta}\frac{k_1 P_{C_4H_{10}}}{k_{-1} + k_{2a} + k_{2b}}. \quad [8]$$

The total number of isobutane molecules colliding with the zeolite surface per second ($k_1 P_{C_4H_{10}}$) is equal to the flow rate ($dn_{C_4H_{10}}/dt$) multiplied by the number of collisions experienced by each isobutane molecule with the surface (Z). In a Knudsen cell, Z is calculated from the ratio of the exposed surface area of the catalyst ($S_{HZ,e}$) to the surface area of the exit aperture (S_{ea}) (1).

$$Z = \frac{S_{HZ,e}}{S_{ea}} \quad [9]$$

The magnitude of $S_{HZ,e}$ is not readily measured. A lower limit to this surface area is estimated by assuming that surfaces within the micropores and external surfaces underneath the top layer of the HZSM-5 are not available for direct adsorption. The remaining exposed surface area is then carefully measured. Values for $S_{HZ,e}$ of 330 mm^2 for Reactor 1 and 160 mm^2 for Reactor 2 were used. Due to the irregular three-dimensional nature of the catalyst particles, the exposed surface area will be higher and some reactant molecules may become trapped between particles or between a particle and the reactor walls. The average collision numbers, listed in Table 1, are used in the calculations, but this choice may cause errors of a factor of ten in the reported Arrhenius preexponential factors. As the collision number is a constant for a particular reactor, the measured activation energy is not affected by the choice of Z. Any change in exposed surface area with temperature, due to coke deposition or catalyst restructuring, will also affect the reported rate constant. For the zeolite catalyst, pressures, and temperatures used in this investigation, these effects should be negligible.

Although the flow rate into the reactor is constant, the total collision frequency is depleted as isobutane is removed due to reaction. The result is a distribution of collision frequencies within the reactor. In order to estimate the collision frequency, the average of the flow rates entering and leaving the reactor is used:

$$\frac{dn_{C_4H_{10}}}{dt} = \frac{I^0_{C_4H_{10}} + I_{C_4H_{10}}}{2\alpha_{C_4H_{10}}}. \quad [10]$$

Here $I^0_{C_4H_{10}}$ and $I_{C_4H_{10}}$ are mass-spectral peak intensities characteristic of isobutane before and after reaction, respectively, and $\alpha_{C_4H_{10}}$ is a calibration factor that converts flow rate to abundance. The activation energy for adsorption of isobutane onto the zeolite surface is taken to be zero in these calculations.

The product flow rate from the reactor is also related to a characteristic mass-spectral peak abundance:

$$I_{Product} = \alpha_{Product}\frac{dn_{Product}}{dt} = \alpha_{Product}\beta\frac{dn_{Product}}{dT}. \quad [11]$$

Substituting Eqs. [9] to [11] into Eq. [8] yields the following rate law in terms of mass spectral intensities:

$$I_{Product} = \frac{\alpha_{Product}S_{HZ,e}}{\alpha_{C_4H_{10}}S_{ea}}\frac{k_{2a\text{ or }2b}}{k_{-1} + k_{2a} + k_{2b}}\frac{\left(I^0_{C_4H_{10}} + I_{C_4H_{10}}\right)}{2}. \quad [12]$$

Provided reactions [R2a] and [R2b] are the dominant surface reaction steps, the ratio of the rate constants for these steps is

$$\frac{k_{2a}}{k_{2b}} = \frac{\alpha_{P,2b}I_{P,2a}}{\alpha_{P,2a}I_{P,2b}}. \quad [13]$$

Here, the terms on the right-hand side of the equation are mass spectral calibration factors and intensities for characteristic product peaks for Reactions [R2a] and [R2b]. Substituting Eq. [13] into Eq. [12] and rearranging to determine the ratio of the isobutane desorption and reaction rate constants,

$$\frac{k_{-1}}{k_{2a\text{ or }2b}} = \frac{\alpha_{P,2a\text{ or }2b}S_{HZ,e}}{\alpha_{C_4H_{10}}S_{ea}}\frac{\left(I^0_{C_4H_{10}} + I_{C_4H_{10}}\right)}{2I_{P,2a\text{ or }2b}} - \frac{\alpha_{P,2a\text{ or }2b}}{\alpha_{P,2b\text{ or }2a}}\frac{I_{P,2b\text{ or }2a}}{I_{P,2a\text{ or }2b}} - 1. \quad [14]$$

The final two terms on the right-hand side of Eq. [14] only affect the smaller rate constant (k_{2a} or k_{2b}), and only if this rate constant is significantly smaller. For isobutane decomposition over HZSM-5 these terms lower the desorption/dehydrogenation ratio by less than 0.1%. The ratio of rate constants $k_{-1}:k_{2a\text{ or }2b}$ have the units (active site coverage/exposed site coverage).

RESULTS

A careful analysis of the mass spectra of isobutane at 0 and 50% conversion indicates that the gas-phase products are methane, propene, isobutene (hydrogen cannot be accurately detected with the current system), and trace amounts of benzene, toluene, and xylene. These low yields of aromatic species have been ignored when determining the cracking and dehydrogenation kinetics. Other possible products, ethane, propane, and *n*-butane, are not apparent in the mass spectra. It is difficult to accurately detect these species at low concentrations, as their mass spectra are similar to the mass spectra of the dominant products. A previous study on isobutane/HZSM-5 reactions also did not report these alkanes (10). The three high-yield products can be characterized by $m/e = 13$ (methane), $m/e = 36$ (propene), and $m/e = 56$ (isobutene). Isobutane contributes to each of these peaks, isobutene makes a small contribution to the abundance of both $m/e = 13$ and $m/e = 36$, and propene makes a small contribution to $m/e = 13$. For isobutane the fractional contributions relative to the $m/e = 58$ peak are measured at the commencement of every temperature-programmed experiment. For the products, separate experiments, using the particular product gas, were carried out over a range of flow rates to determine the relative abundances. Listed in Table 2 are the measured fractional abundances of the reactant and each product for the respective peaks. These fractions have been used to correct the measured abundances.

For the reactant gas, the mass-spectral conversion factor ($\alpha_{C_4H_{10}}$ (abundance s mole^{-1})) is readily determined at the commencement of a temperature-programmed experiment, when reaction is negligible. The average abundance of the $m/e = 58$ peak is simply divided by the measured molecular flow rate. Separate experiments are required to determine the product conversion factors using pure product samples. Day-to-day fluctuations in these product conversion factors are accounted for by comparison with changes in the $m/e = 58$ conversion factor. Mean conversion factors are included in Table 2.

Ten temperature-programmed experiments were carried out on the isobutane/HZSM-5 catalytic reaction. Both reactors were employed, flow rates ranged from 1.29×10^{14} molecules s^{-1} to 2.90×10^{15} molecules s^{-1}, and the heating rate was varied from 2 to 10°C min^{-1}. Some problems were experienced in the interpretation of 10°C min^{-1} experiments as the heating rate dropped off rapidly beyond 450°C. For 5°C min^{-1} the heating rate decreased from ca. 490°C, so data beyond this temperature were discarded. The significance of the reactor, flow rate, and heating rate is that the larger the collision frequency and heating rate the higher the sensitivity of the experiment because the abundance of the mass spectral peaks is largest. The most sensitive temperature-programmed experiment had a total collision frequency with the catalyst of 4.64×10^{19} collisions s^{-1} and was undertaken at 5°C min^{-1} in Reactor 1. A typical temperature-programmed reaction profile for the four mass spectral peaks is plotted in Fig. 2, where the heating rate is 2°C min^{-1} and the initial flow rate into Reactor 1 is 4.73×10^{14} molecules s^{-1}. Isobutane declines, while isobutene, propene, and methane increase under these conditions from ca. 380°C. Product formation is not exponential, over the entire temperature range, due to the decrease in isobutane coverage resulting from the decrease in reactant pressure and surface reaction.

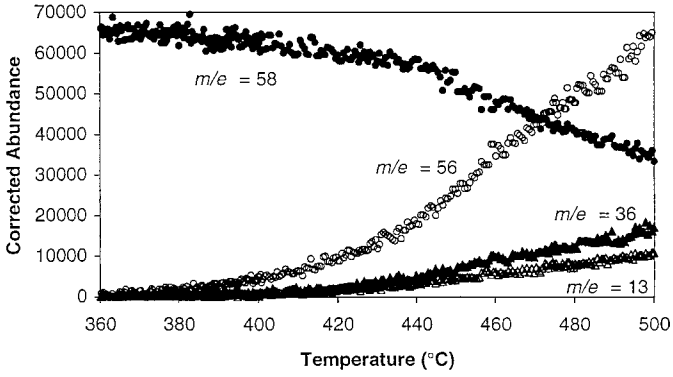

FIG. 2. Corrected mass-spectral abundances for isobutane decomposition (●, $m/e = 58$), isobutene formation (○, $m/e = 56$), propene formation (▲, $m/e = 36$), and methane formation (△, $m/e = 13$) during TPRS in Reactor 1, with an initial isobutane flow rate of 4.73×10^{14} molecules s^{-1} and a heating rate of 2°C min^{-1}.

TABLE 2

Calibration Factors for the Mass Spectrometer

	Isobutane	Isobutene	Propene	Methane
I_{56}/I_{58}	0.1377 ± 0.0028			
I_{36}/I_{58}	0.0461 ± 0.0017			
I_{13}/I_{58}	0.0610 ± 0.0008			
I_{36}/I_{56}		0.0115 ± 0.0011		
I_{13}/I_{56}		0.0090 ± 0.0029		
I_{13}/I_{36}			0.0068 ± 0.0022	
$\alpha(I$ s/moles)	$1.7 \pm 0.8 \times 10^{14}$	$1.8 \pm 0.8 \times 10^{15}$	$1.1 \pm 0.5 \times 10^{14}$	$1.6 \pm 0.8 \times 10^{14}$

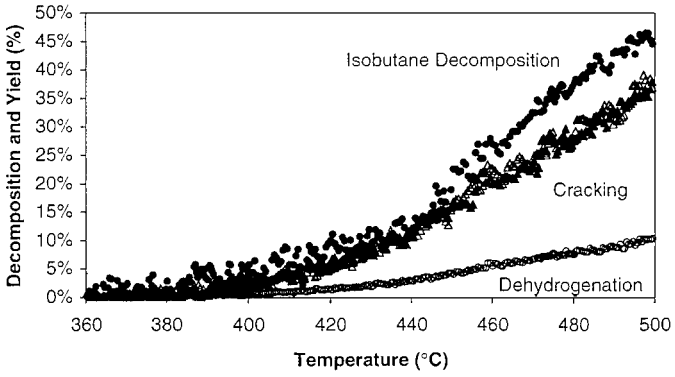

FIG. 3. Percentage isobutane decomposition and cracking and dehydrogenation yields. Experimental points refer to isobutane decomposition (●), isobutene formation (○), propene formation (▲), and methane formation (△) during TPRS in Reactor 1, with an initial isobutane flow rate of 4.73×10^{14} molecules s^{-1} and a heating rate of 2°C min^{-1}.

The fractional decomposition of isobutane and fractional yields of products are given by

$$f_{\text{Decomposition}} = \frac{I^0_{C_4H_{10}} - I_{C_4H_{10}}}{I^0_{C_4H_{10}}} \quad [15]$$

$$f_{\text{Yield}} = \frac{\alpha_{C_4H_{10}} I_{\text{Product}}}{\alpha_{\text{Product}} I^0_{C_4H_{10}}} \quad [16]$$

In Fig. 3 these fractions are plotted as a percentage for the reaction profile shown in Fig. 2. Isobutane approaches 50% conversion at 500°C, and clearly the cracking reaction, formation of propene and methane, dominates over dehydrogenation.

A plot of the natural logarithm of the right-hand side of Eq. [14], which contains all experimentally observed or estimated quantities, against $1/RT$ produces a straight line with slope equal to $-E_{-1} + E_{2a \text{ or } 2b}$ and an intercept of $\ln(A_{-1}/A_{2a \text{ or } 2b})$. This plot is shown in Fig. 4 for the temperature-programmed experiment performed in Reactor 1 with a heating rate of 2°C min^{-1} and an initial

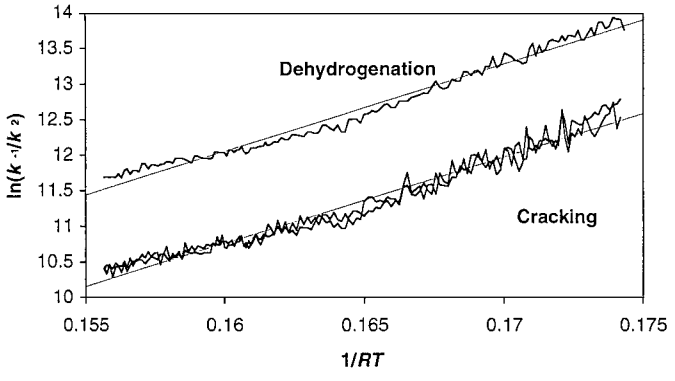

FIG. 4. Arrhenius-type plots of $\ln(k_{-1}/k_2)$ against $1/RT$ for isobutane dehydrogenation and cracking over HZSM-5.

TABLE 3

Rate Parameters Determined for the HZSM-5 Cracking and Dehydrogenation of Isobutane

	$\log_{10}(\beta A_{-1}/A_2)$ ($\log_{10}(°Cs^{-1})$)	$\log_{10}(A_2/\beta)$ ($\log_{10}(°C^{-1})$)	E_{-1}–E_2 (kJ mol^{-1})	E_2 (kJ mol^{-1})
Cracking	-5.30 ± 0.12	17.3 ± 2.0	-121.7 ± 1.7	170 ± 6
Dehydrogenation	-4.81 ± 0.10	16.8 ± 2.0	-123.4 ± 1.4	172 ± 6

isobutane flow rate of 4.73×10^{14} molecules s^{-1}. The average Arrhenius preexponential factors and activation energies with corresponding standard deviations determined from all temperature-programmed experiments on this isobutane/HZSM-5 system are listed in Table 3.

DISCUSSION

It is clear from Figs. 3 and 4 that the formation rate and yield of cracking products are significantly greater than those of dehydrogenation products. This distinction has been previously reported for isobutane reactions over HZSM-5 and USY, as well as for *n*-butane over HZSM-5 (6, 10). The difference in rate constants for the two pathways is

$$\frac{k_{2a}}{k_{2b}} = 3.1 \pm 1.7 \times \exp(1.7 \pm 3.1 \text{ kJ mol}^{-1}/RT).$$

Taking into account experimental errors, activation energies for the two channels are indistinguishable. This equivalence is in agreement with proton affinities for carbon attached to secondary carbon and hydrogen attached to a tertiary carbon, calculated by Collins and O'Malley (21). However, the magnitude of the preexponential factor is significant, despite the relatively large errors. The ratio of preexponential factors may represent the difference in reaction path degeneracy of the initial reaction steps for the two pathways.

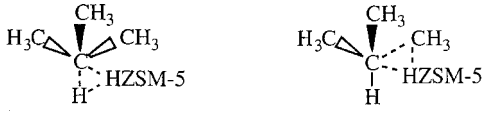

Dehydrogenation Cracking

For dehydrogenation, only one hydrogen, attached to a tertiary carbon, is available for attack by acidic zeolite sites, while three identical carbon–carbon bonds are available for cracking. Hence a factor of three difference in the preexponential factors is observed. This suggests that initial attack by Brønsted acid sites on the HZSM-5 is rate determining. Here it is assumed that the concentration of Lewis acid sites on the zeolite surface is neglible (10, 22).

The preexponential factors for Reactions [R2a] and [R2b] can be estimated by allowing for the isobutane desorption preexponential factor. Pitt *et al.* (23) have shown that for physisorbed systems these factors should be in the range 10^{11}–10^{13} s^{-1}. Listed in Table 3 are cracking and dehydrogenation preexponential factors that have been determined assuming $A_{-1} = 10^{12\pm1}$ s^{-1}. The resultant cracking and dehydrogenation preexponential factors are larger than typical factors reported for unimolecular gas-phase reactions where entropy changes between the reactant and the transition state are negligible (24). Implicit in the cracking and dehydrogenation factors is that the coverage of external sites is equal to the coverage of active sites. Large preexponential factors suggest that this assumption is not valid. That is, the coverage of active sites within the pores of the HZSM-5 is much less than the coverage of the external surface. This indicates that surface diffusion to a fraction of the active sites is not rapid and a steady-state concentration is not reached. Perhaps access to some sites is limited. An alternative explanation for the large preexponential factors is that the entropy when transforming from isobutane to the transition state is increasing. Such an entropy increase may be due to the introduction of an extra proton from HZSM-5 to form a carbonium ion, resulting in extra stretching and bending motions. This effect, however, is likely to be only a minor contributor to the preexponential factor.

Cracking and dehydrogenation activation energies may be calculated by correcting for the enthalpy of adsorption of isobutane. For isobutane on HZSM-5 and silicalite this value has been determined using a range of methods (18, 19). Reported magnitudes of the enthalpy are independent of the Si/Al ratio and vary from −42 to −56.5 kJ mol^{-1}. As the activation energy for adsorption is taken to be zero, a mean value of -48.7 ± 4.7 kJ mol^{-1} is used for E_{-1}, and hence E_{2a} is estimated to be 170 ± 6 kJ mol^{-1} and E_{2b} is 172 ± 6 kJ mol^{-1}. Ab initio quantum chemical calculations have been used by Kazansky *et al.* (25) to predict these energies for isobutane on various H/O/Al clusters. Here magnitudes of 241 kJ mol^{-1} for cracking and 279 kJ mol^{-1} for dehydrogenation were reported, which are 71 and 107 kJ mol^{-1} higher than our values. Also the theoretical difference between the two reaction channels is 38 kJ mol^{-1}, while we have determined a negligible difference. This poor comparison between theory and experiment may be due to the acidity of the theoretical cluster relative to HZSM-5, or it may indicate that alternate reaction dynamics are occurring for one or both channels.

Experimental activation energies reported in the literature for these two reaction channels for isobutane and *n*-butane over zeolites are listed in Table 4. These are apparent values and represent a combination of the adsorption enthalpy ($E_1 - E_{-1}$) and the intrinsic reaction activation energies (E_2). A direct comparison can be made with the values obtained by Narbeshuber *et al.* (10) for isobutane over HZSM-5. For cracking, the activation energies are similar (125 cf. 121.7 kJ mol^{-1}), but for dehydrogenation the difference is large (100 cf. 123.4 kJ mol^{-1}). The low dehydrogenation activation energy is surprising as Narbeshuber *et al.* also indicate that cracking occurs at a higher rate than dehydrogenation. Experimental work by Corma *et al.* (14) on isobutane cracking and dehydrogenation over USY zeolites have determined an increase of 9 kJ mol^{-1}, which also disagrees with the decrease of 25 kJ mol^{-1} determined by Narbeshuber *et al.* The same authors (10) and Krannila *et al.* (26) have analyzed the kinetics of *n*-butane decomposition over HZSM-5. The former study reported a large decrease of 20 kJ mol^{-1} between the two channels, while an increase of 7 kJ mol^{-1} is determined by Krannila *et al.* Theoretical proton affinities indicate that hydrogen attached to secondary carbon has a 34 kJ mol^{-1} lower proton affinity than carbon attached to primary carbon (21). That is, the values are larger than and opposite in sign to those expected from the Narbeshuber *et al.* (10) values.

The Krannila *et al.* (26) activation energy for cracking of *n*-butane over HZSM-5 is 20 kJ mol^{-1} higher than our isobutane value, while for dehydrogenation of *n*-butane the energy is 26 kJ mol^{-1} higher. Isobutane has a tertiary carbon, which is expected to lower the intrinsic activation energy. Collins and O'Malley (21) predict proton affinity differences for the respective C–C and C–H bonds of 42 and 76 kJ mol^{-1}, respectively, but note that their calculations of absolute activation energies differ from the Krannila *et al.* experimental values by an excess of 65 kJ mol^{-1}.

TABLE 4

Apparent Rate Parameters for Zeolite Cracking and Dehydrogenation of Isobutane and *n*-Butane

Reactant	Zeolite	$E_1 - E_{-1} + E_2$ (kJ mol^{-1})	
Cracking			
Isobutane	HZSM-5 (Si/Al = 16.5)	121.7 ± 1.7	this work
Isobutane	HZSM-5 (Si/Al = 35)	125	(10)
n-Butane	HZSM-5 (Si/Al = 35)	135	(10)
n-Butane	HZSM-5 (Si/Al = 35)	142	(26)
Isobutane	USY (Si/Al = 172)	157 ± 19	(14)
Isobutane	USY (Si/Al = 5.2)	170 ± 2	(14)
Dehydrogenation			
Isobutane	HZSM-5 (Si/Al = 16.5)	123.4 ± 1.4	this work
Isobutane	HZSM-5 (Si/Al = 35)	100	(10)
n-Butane	HZSM-5 (Si/Al = 35)	115	(10)
n-Butane	HZSM-5 (Si/Al = 35)	149	(26)
Isobutane	USY (Si/Al = 172)	166 ± 22	(14)
Isobutane	USY (Si/Al = 5.2)	117 ± 3	(14)

CONCLUSION

Accurate kinetic parameters have been obtained for the cracking and dehydrogenation of isobutane over HZSM-5

in a low-pressure reactor. The dimensions of the reaction cell, particularly the effective area of the exit aperture, and the isobutane flow rate into the reactor, as well as adsorption and intrinsic reaction, control the rate of product formation. Under the low-pressure conditions, gas/gas collisions, isobutane coverage on HZSM-5, and hence secondary reactions are minimized.

Two dominant reaction channels—cracking and dehydrogenation—are observed, although trace amounts of benzene, toluene, and xylene are apparent in the mass spectra. Cracking, characterized by propene and methane products, dominates over dehydrogenation, which is characterized by isobutene. The ratio of the rate constant for isobutane desorption to the rate constants of isobutene, propene, and methane formation is determined from the reactant and product mass-spectral abundances, mass spectral calibration factors, and the collision frequency with the zeolite surface. The temperature dependence of this ratio for cracking is

$$\frac{k_{-1}}{k_{2a}}\,(^{\circ}\mathrm{Cs}^{-1}) = 10^{-5.30\pm0.12}\exp(121.7 \pm 1.7\,\mathrm{kJ\ mol}^{-1}/RT),$$

and for dehydrogenation it is

$$\frac{k_{-1}}{k_{2b}}\,(^{\circ}\mathrm{Cs}^{-1}) = 10^{-4.81\pm0.10}\exp(123.4 \pm 1.4\,\mathrm{kJ\ mol}^{-1}/RT).$$

Similarity in activation energies is in agreement with predicted proton affinities (21) for the respective C–C and C–H bonds involved in the reaction pathways. Differences between these activation energies and energies reported in the literature on similar systems are either insignificant or can be explained by anomalies in the literature values or by accounting for differences in the reactant and substrate. Preexponential factors suggest that surface diffusion to some active sites is slow, resulting in a smaller coverage of active sites than coverage of the external or exposed surface.

ACKNOWLEDGMENTS

Financial support from the Australian Research Council is gratefully acknowledged. Sun Yanping is also appreciative of UNERS and OPRS awards.

REFERENCES

1. Golden, D. M., Spokes, G. N., and Benson, S. W., *Angew. Chem.* **12**, 534–546 (1973).
2. Fenter, F. F., and Rossi, M. J., *J. Phys. Chem. A* **101**, 4110–4113 (1997).
3. Caloz, F., Fenter, F. F., Tabor, K. D., and Rossi, M. J., *Rev. Sci. Instrum.* **68**, 3172–3179 (1997).
4. Niemantsverdriet, J. W., "Spectroscopy in Catalysis." VCH, Weinheim, 1995.
5. Wojciechowski, B. W., and Asprey, S. P., *Appl. Catal. A Gen.* **190**, 1–24 (2000).
6. Jentoft, F. C., and Gates, B. C., *Topics Catal.* **4**, 1–13 (1997).
7. Kazanzky, V. B., *Catal. Today* **51**, 419–434 (1999).
8. Williams, B. A., Babitz, S. M., Miller, J. T., Snurr, R. Q., and Kung, H. H., *Appl. Catal. A Gen.* **177**, 161–175 (1999).
9. Sommer, J., Habermacher, D., Hachoumy, M., Jost, R., and Reynaud, A., *Appl. Catal. A Gen.* **146**, 193–205 (1996).
10. Narbeshuber, T. F., Brait, A., Seshan, K., and Lercher, J. A., *J. Catal.* **172**, 127–136 (1997).
11. Corma, A., and Orchilles, A. V., *Microporous Mesoporous Mater.* **35–36**, 21–30 (2000).
12. Ward, J. W., *J. Catal.* **9**, 225–236 (1967).
13. Haag, W. O., and Dessau, R. M., *in* "Proceedings, 8th International Congress on Catalysis, Berlin, 1984," Vol. 2, pp. 305–317. Dechema, Frankfurt-am-Main, 1984.
14. Corma, A., Miguel, P. J., and Orchilles, A. V., *J. Catal.* **145**, 171–180 (1994).
15. Iczkowski, R. P., Margrave, J. L., and Robinson, S. M., *J. Phys. Chem.* **67**, 229–233 (1963).
16. Reid, R. C., Prausnitz, J. M., and Poling, B. E., "The Properties of Gases and Liquids." McGraw–Hill, New York, 1987.
17. Do, D. D., "Adsorption Analysis: Equilibria and Kinetics." Imperial College Press, London, 1998.
18. Nijhuis, T. A., van-den-Broeke, L. J. P., Linders, M. J. G., Makkee, M., Kapteijn, F., and Moulijn, J. A., *Catal. Today* **53**, 189–205 (1999).
19. Keipert, O. P., and Baerns, M., *Chem. Eng. Sci.* **53**, 3623–3634 (1998).
20. Trout, B. L., Chakraborty, A. K., and Bell, A. T., *Chem. Eng. Sci.* **52**, 2265–2276 (1997).
21. Collins, S. J., and O'Malley, P. J., *Topics Catal.* **6**, 151–161 (1998).
22. Haag, W. O., Lago, R. M., and Weisz, P. B., *Nature* **309**, 589–591 (1984).
23. Pitt, I. G., Gilbert, R. G., and Ryan, K. R., *J. Chem. Phys.* **102**, 3461–3473 (1995).
24. Benson, S. W., "Thermochemical Kinetics." Wiley, New York, 1976.
25. Kazansky, V. B., Frash, M. V., and Santen, R. A. V., *Appl. Catal. A* **146**, 225–247 (1996).
26. Krannila, H., Haag, W. O., and Gates, B. C., *J. Catal.* **135**, 115–124 (1992).